Supporting Information

Atomic Origins of Strong Metal-Support Interaction in Silica Supported Catalysts

Feng Yang[#], Haofei Zhao[#], Wu Wang[#], Lei Wang, Lei Zhang, Tianhui Liu, Jian Sheng,

Sheng Zhu, Dongsheng He, Lili Lin, Jiaqing He*, Rongming Wang* and Yan Li*
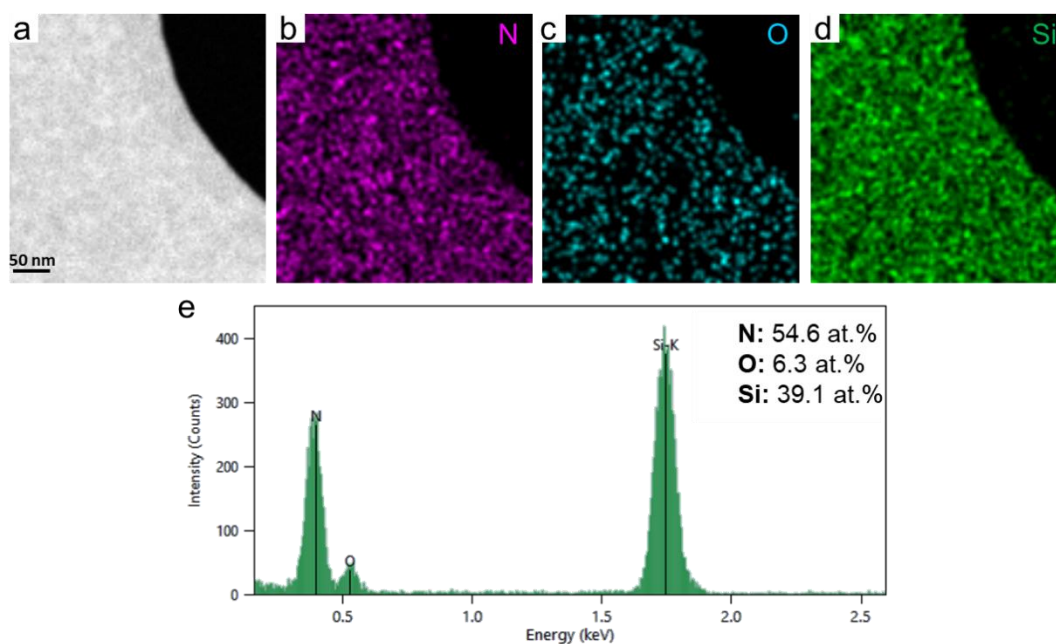
Figure S1. **a–d**, STEM image (**a**) and EDX elemental mapping on pristine ETEM chip showing a thin-film of SiO_2 on SiN_x membrane (**b–d**). **e**, Corresponding EDX spectrum. The relative abundance of N, O, and Si were also shown.

Table S1. Quantitative analysis of N, O, and Si by EDX mapping on six regions of pristine ETEM chip.

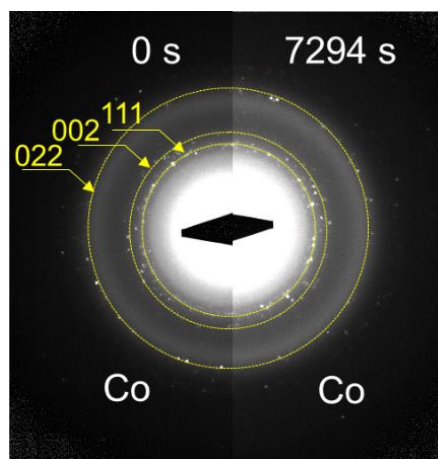| Region No.	N (at.%)	O (at.%)	Si (at.%)
1	54.6	6.5	39.9
2	54.1	6.0	39.9
3	54.1	5.4	40.5
4	53.7	5.8	40.5
5	54.4	6.6	39.0
6	53.6	6.0	40.4
Average	54.0	6.0	40.0

Figure S2. SAED patterns of Co nanoparticle before (0 s) and after annealing (7294 s). The SAED was acquired *in-situ* at 750 °C.
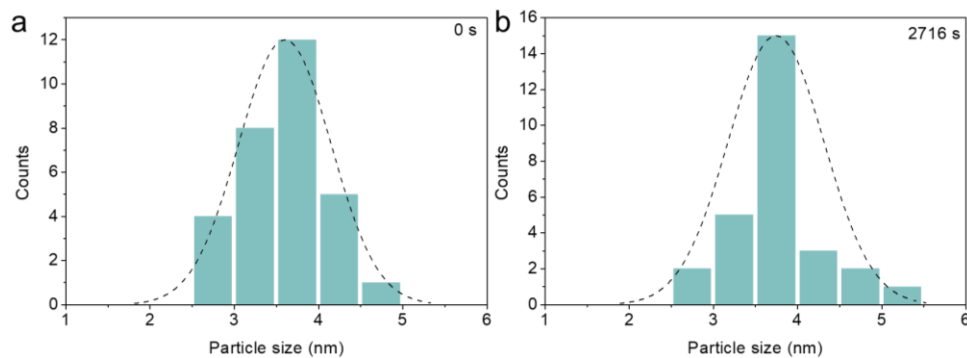

Figure S3. Size distribution of Co nanoparticles on carbon substrate derived from ETEM images acquired at relative time: **a**, 0 s, **b**, 2716 s.
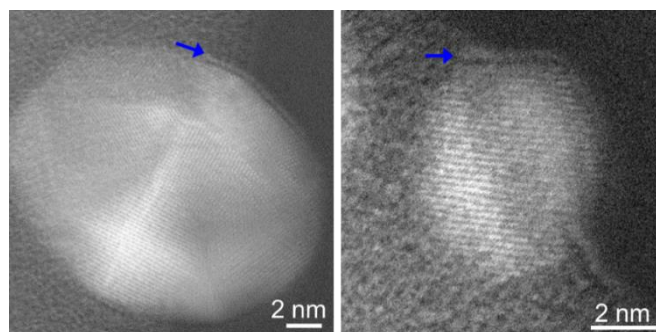
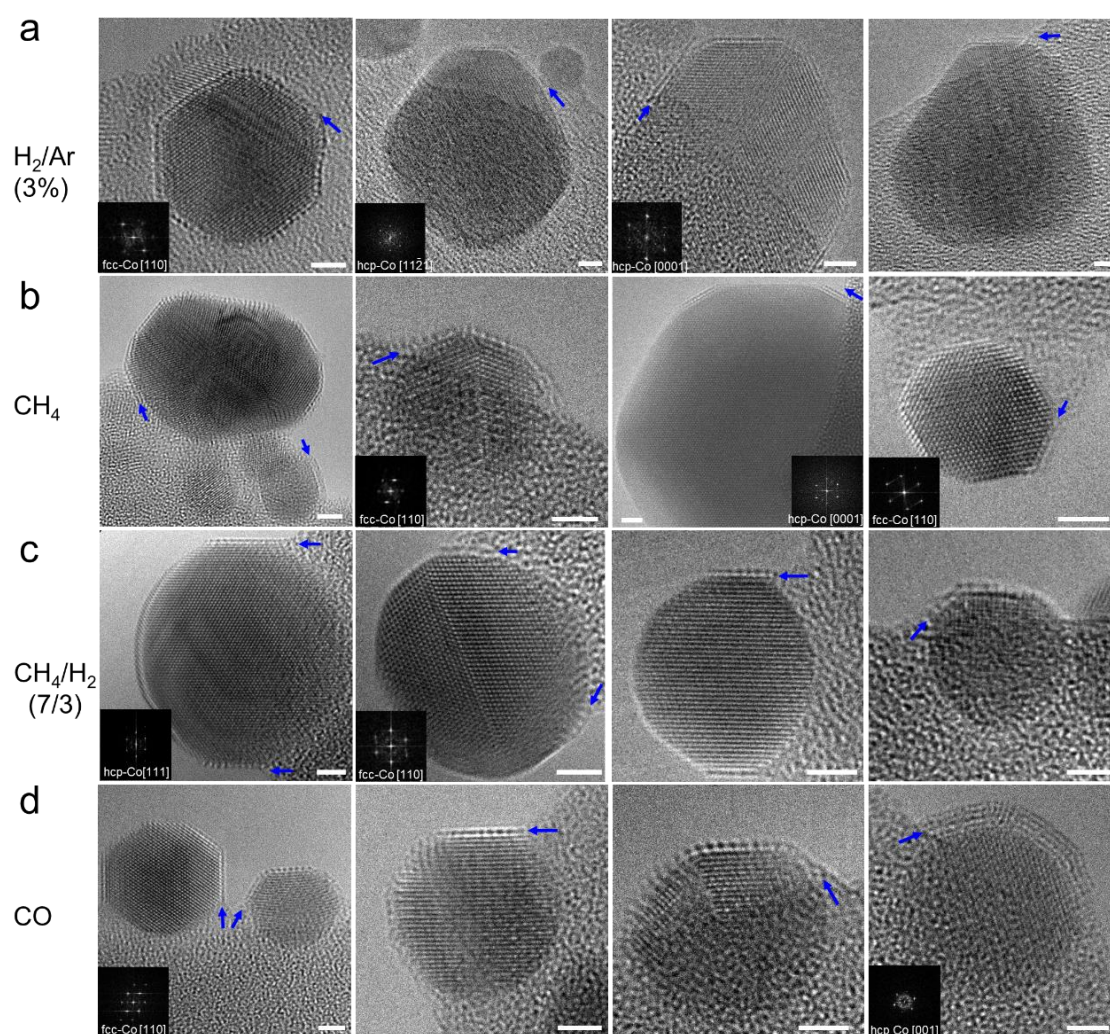**Figure S4**. *In-situ* HAADF-STEM images of Co nanoparticles with overlayer on the edge of substrate under 3% H$_2$/Ar.

Figure S5. ETEM images of Co nanocrystals with overlayer obtained in different conditions at 750 °C: **a**, 3% H$_2$/Ar. **b**, CH$_4$. **c**, CH$_4$/H$_2$ (v/v=7/3), **d**, CO. The overlayer were indicated by arrows. All scale bars: 2 nm. Typical FFT patterns of fcc and hcp-Co were also shown in TEM images.
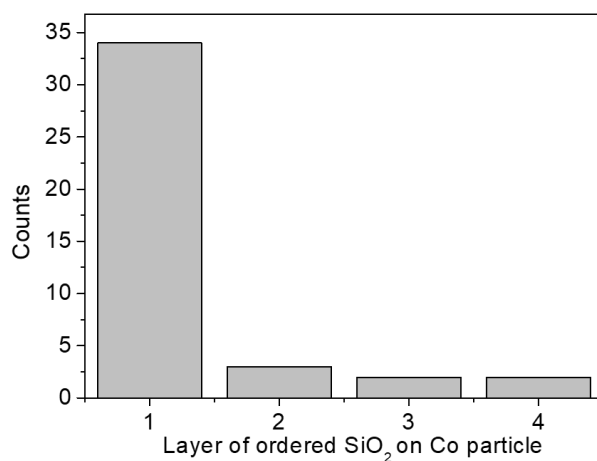
Figure S6. Statistical analysis of layer of ordered SiO_2 covered on Co nanoparticles derived from TEM images.
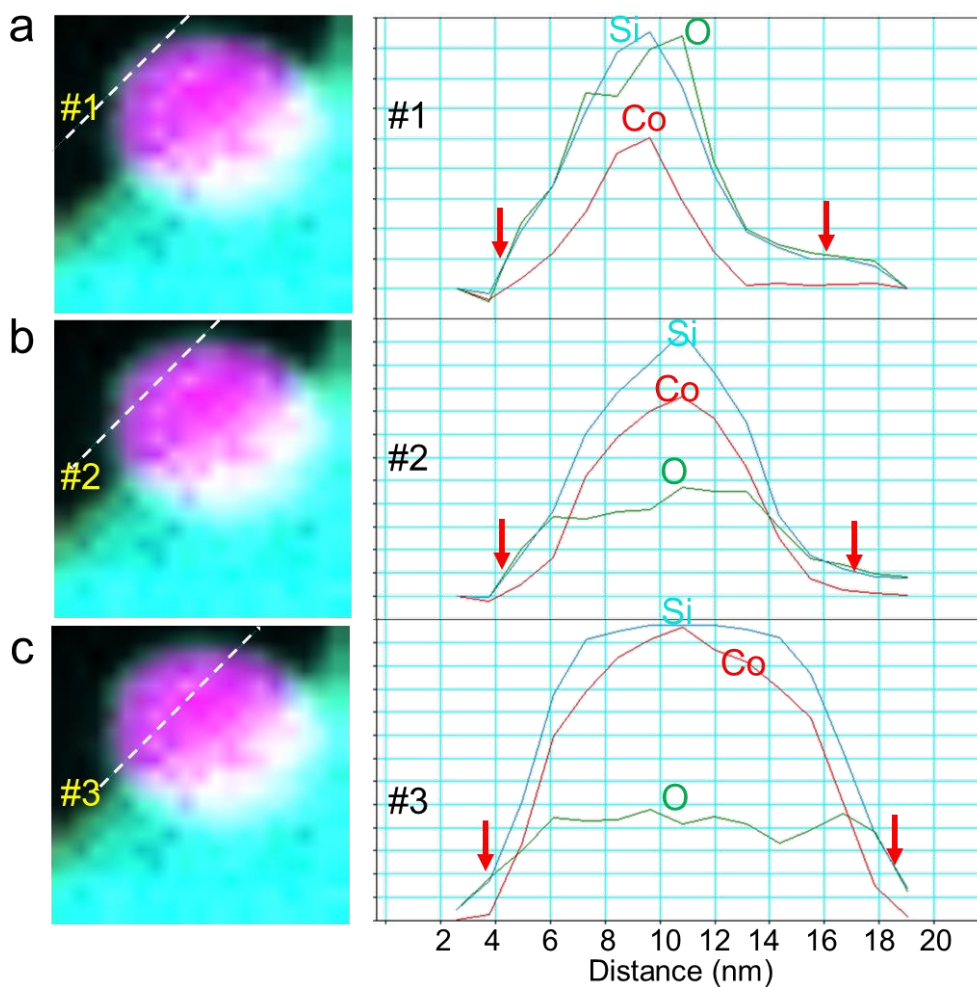

Figure S7. **a–c**, *In-situ* EELS elemental mapping of Si, O, Co on the same Co particle as shown in Figure 2a. Corresponding line scan profiles of EELS across the Co-overlayer indicated with #1–#3 in (**a–c**).
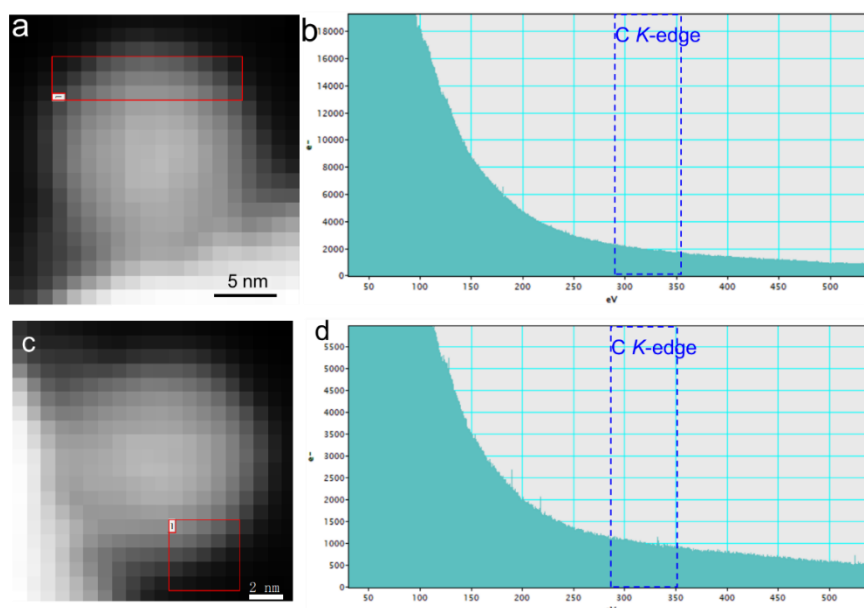
Figure S8. **a**, **c**, *In-situ* STEM-EELS image of a Co nanoparticles on SiO_2/SiN_x substrate annealing under H_2/CH_4 (**a**) and CO (**c**) conditions. The particle in (**a**) is the same as shown in Figure 2a. **b**, **d**, Corresponding EELS spectrum of C K-edge obtained at the surface of Co nanoparticle.

The inversed FFT (IFFT) formed using spots of SiO_2 in corresponding FFT matched well with the simulated TEM contrast of quartz SiO_2 [$10\bar{1}$] (Fig. S9d–f).
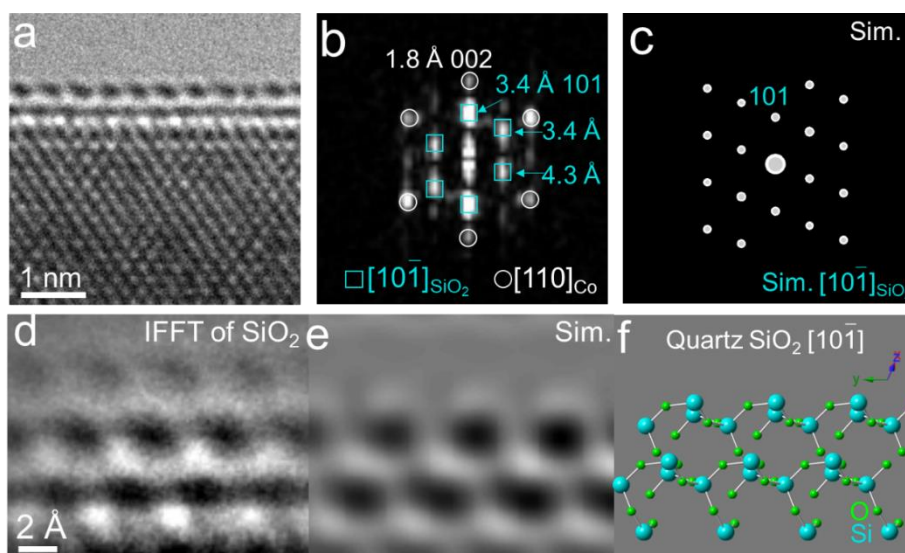

Figure S9. **a**, ETEM image of SiO_2-Si-Co interface. **b**, FFT pattern as shown in Figure 3b. **c**, Simulated electron diffraction pattern of quartz SiO_2 along [$10\bar{1}$] direction. **d–f**, IFFT formed using spots of SiO_2 in corresponding FFT (**d**) and simulated TEM image

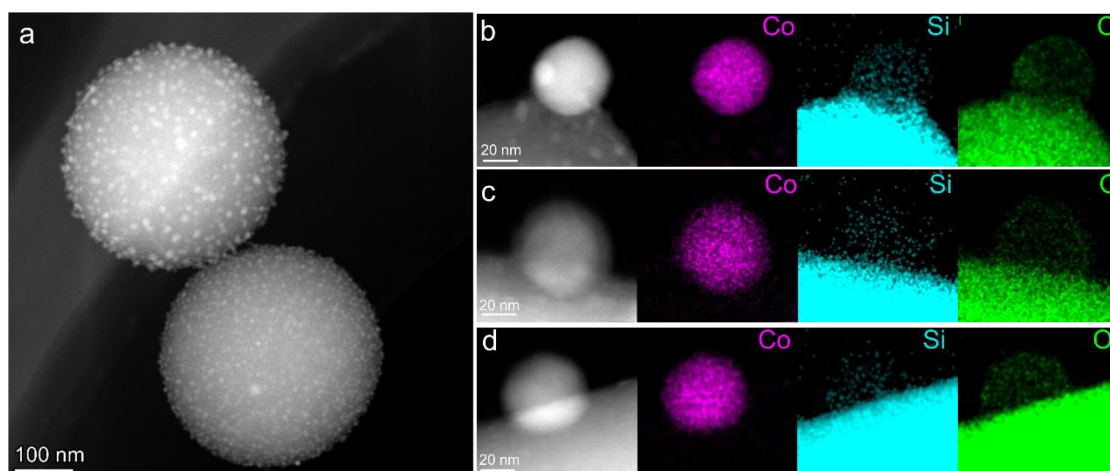(**e**) obtained from atomic structure model of quartz SiO_2 $[10\bar{1}]$ (**f**).

Figure S10. **a–d**, HAADF-STEM images and EDX elemental mapping of Co/SiO_2 after annealing under 10% H_2/Ar at 750 °C for 6 h.
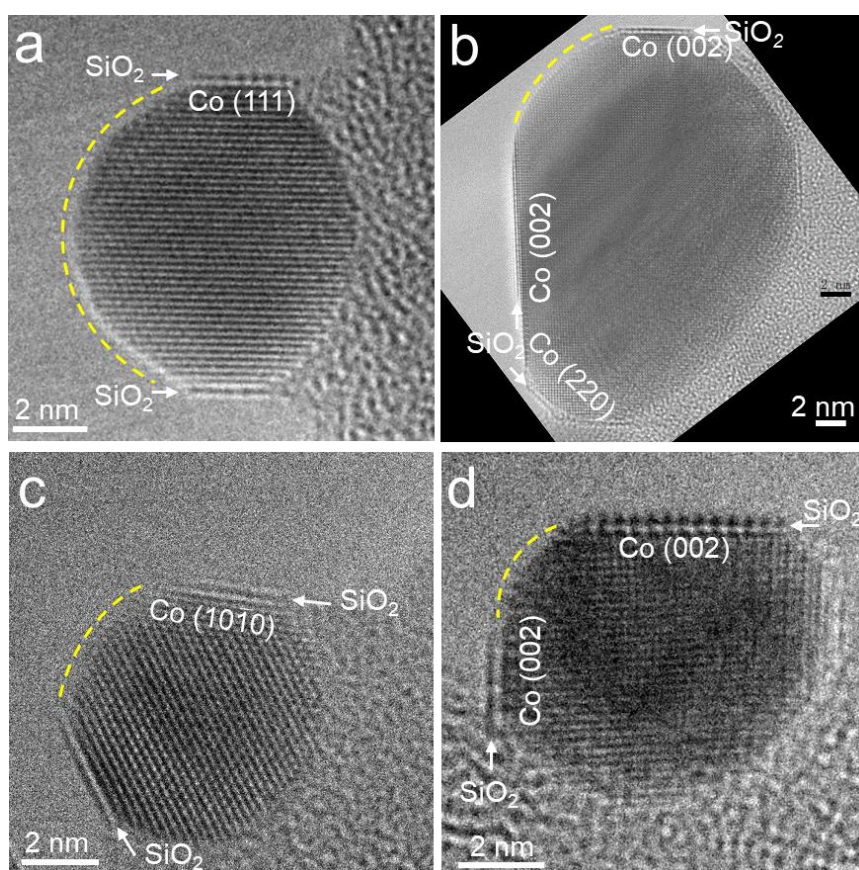

Figure S11. **a–d**, Single-shot ETEM images of Co nanocrystals with SiO_2 overlayer on flat facet with low index. The round surface consisting of high index crystal planes was marked by dashed line.
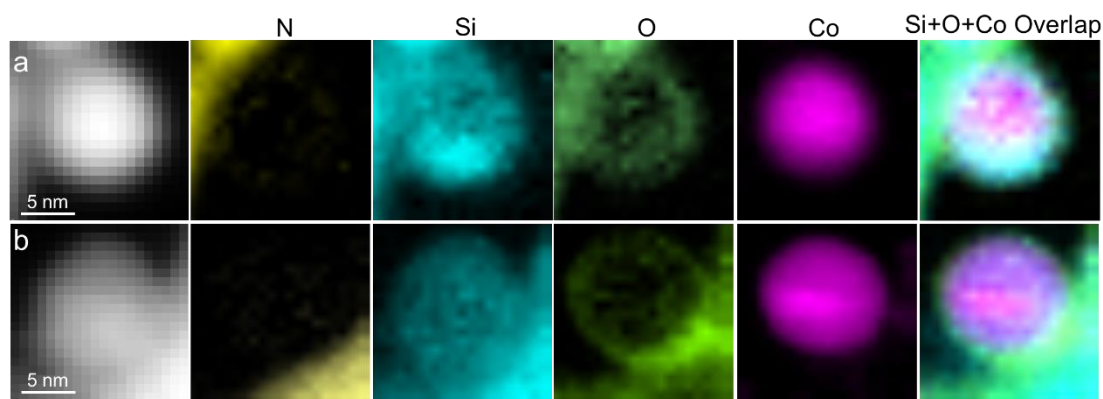
Figure S12. *In-situ* **STEM-EELS characterization**. **a**, **b**, STEM-EELS images of two Co nanoparticles on SiO_2/SiN_x in 3% H_2/Ar (50 Pa) at 750 °C. Corresponding EELS elemental mapping of N K-edge, Si $L_{2,3}$-edge, O K-edge, Co $L_{2,3}$-edge, and their combinatial images.
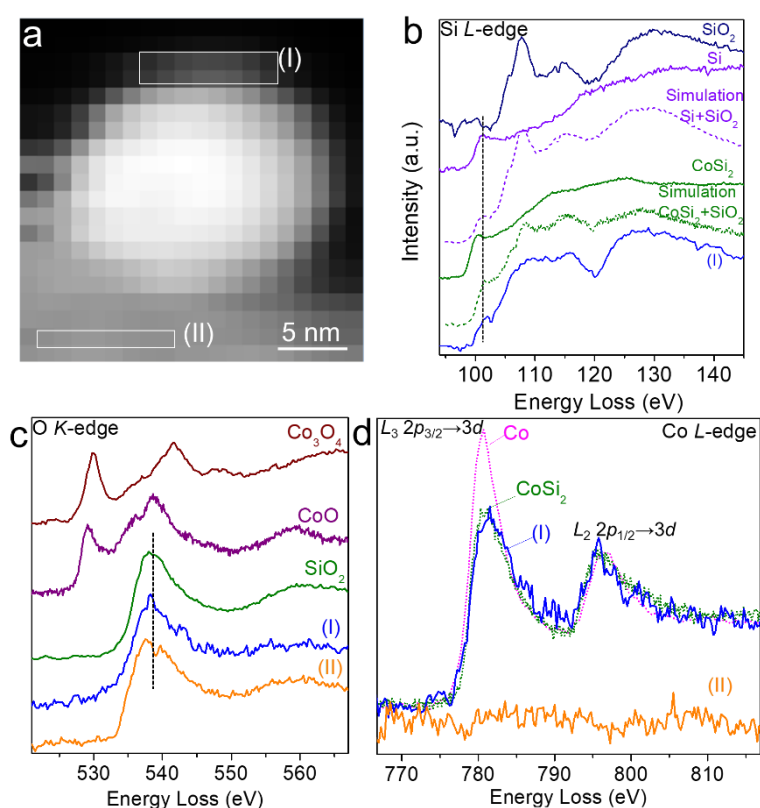

Figure S13. *In-situ* **STEM-EELS characterization**. **a**, SETM-EELS spectrum image showing a Co nanoparticle on SiO_2/SiN_x substrate in 3% H_2/Ar at 750 °C. **b**–**d**, EELS spectra extracted from (**a**, regions I and II), showing Si (**b**), O (**c**), and Co (**d**) signals from nanoparticle and substrate. Commercial Si, SiO_2, and $CoSi_2$ were used as referenced samples, CoO, Co_3O_4, Co, and Si_3N_4 from EELS database were used. All

the spectra were calibrated by using the zero-loss peak (0 eV). The EELS spectra of Co L-edge were normalized by the energy loss peak of Co L_2-edge.
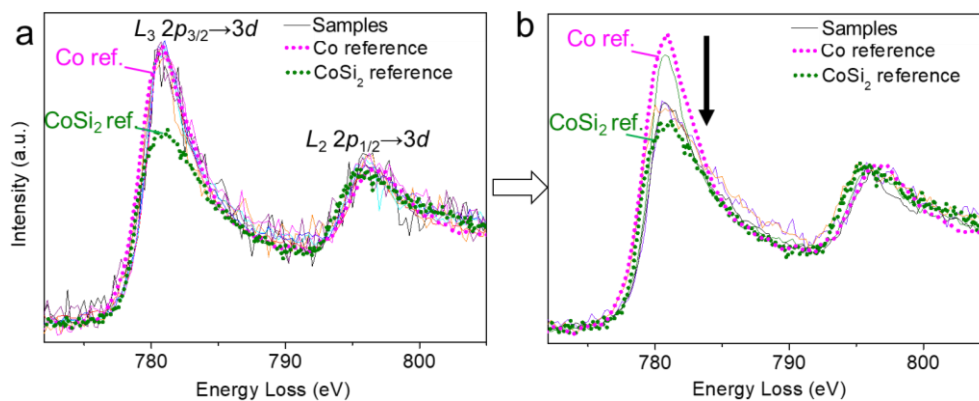

Figure S14. a, **b**, *In-situ* EELS Co $L_{2,3}$ spectra of Co-SiO$_2$ before (**a**) and after (**b**) order-to-disorder transition of SiO$_2$. The EELS spectra of different Co-SiO$_2$ nanoparticles and Co and CoSi$_2$ references were calibrated by the zero-loss peak (0 eV) and then normalized by the energy loss peak of Co L_2-edge.
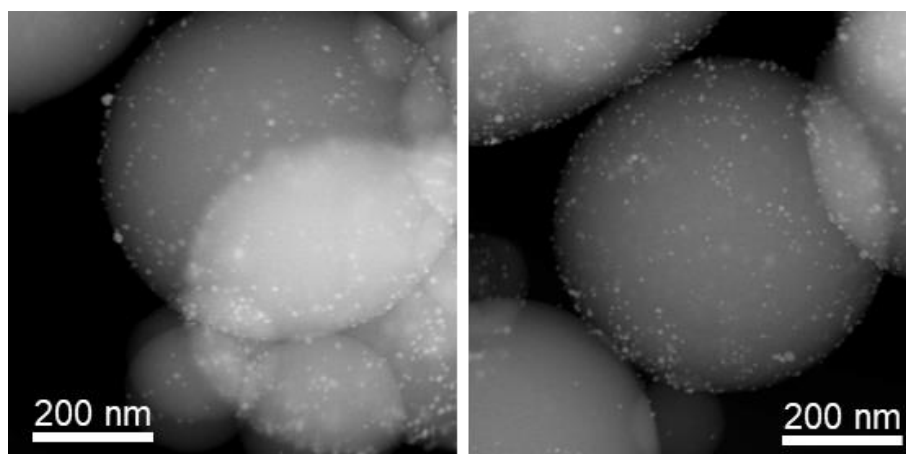

Figure S15. HAADF-STEM images of as-prepared Pt nanoparticles supported on SiO$_2$ spheres.
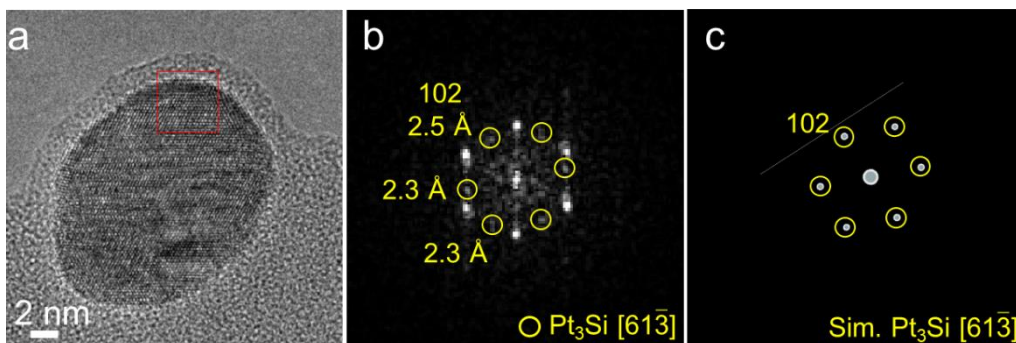
Figure S16. **a**, High-resolution TEM image of Pt nanoparticle supported on SiO_2. **b**, FFT derived from region marked in (**a**). **c**, Simulated FFT of Pt_3Si [$61\bar{3}$].

Table S2. Active surface area of Pt/SiO_2 catalyst annealed at 500-900 $^\circ$C, which was characterized by CO adsorption. The loading amount of Pt was controlled to 3 wt% of the support.

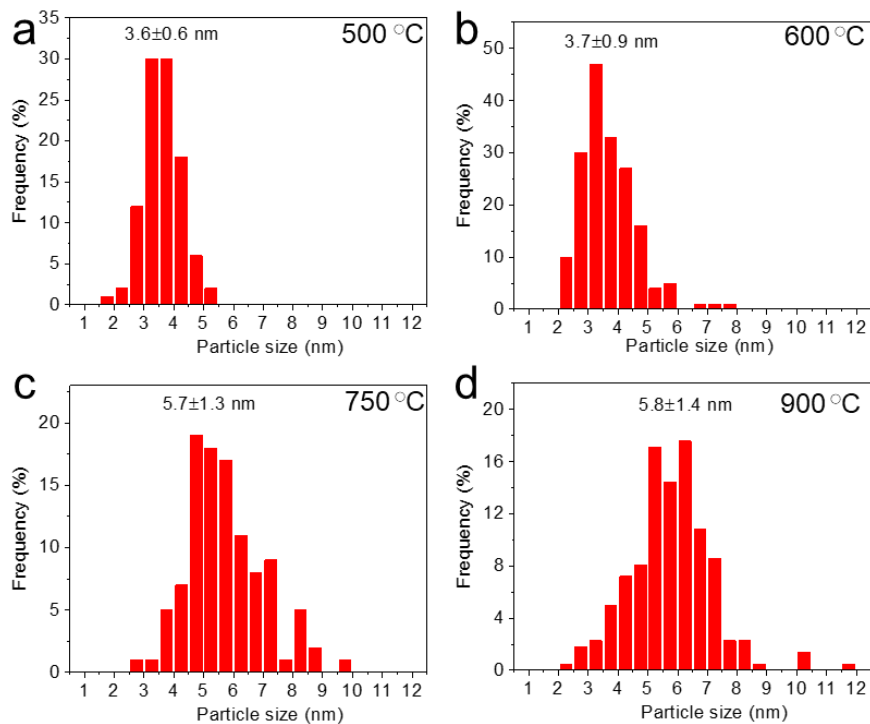| Catalyst reduction temperature ($^\circ$C)	Active Pt surface area (m^2/g-cat)
500	0.93
600	4.15
750	3.91
900	1.73

Figure S17. Distributions of Pt catalyst size calcined at 500 (**a**), 600 (**b**), 750 (**c**), and 900 °C (**d**). The Pt catalyst was supported on SiO$_2$ spheres. The averaged Pt particle size was also shown in each panel.
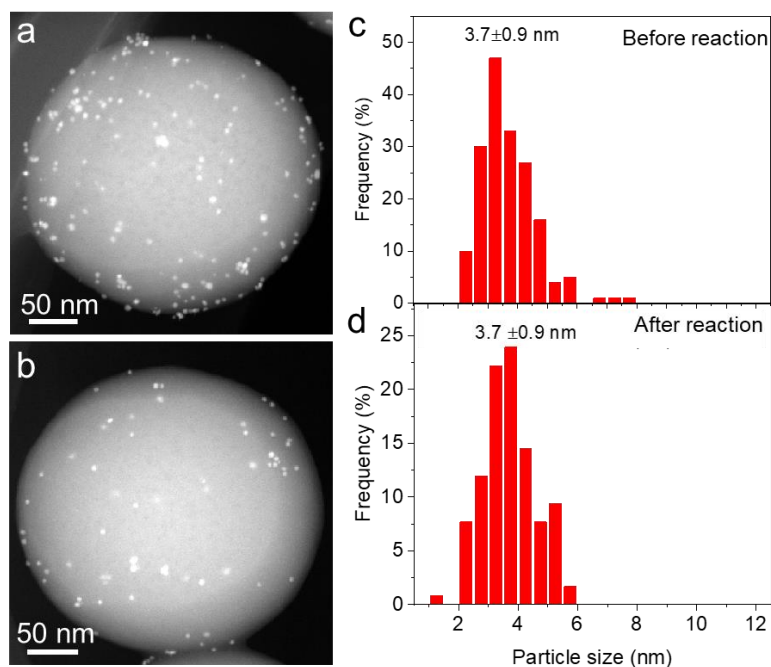

Figure S18. **a**, **b**, TEM images of Co/SiO$_2$ catalyst after hydrogenation reaction. **c**, **d**, Size distribution of Pt nanoparticles before (**c**) and after (**d**) reaction. Panel (**c**) is the same as in Fig. S17b.